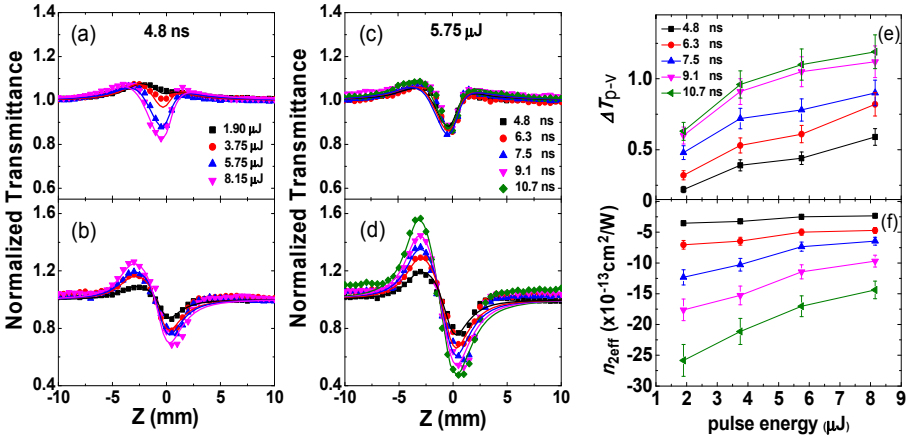

Fig. 2. Open-aperture Z-scan curves (a) and NLR Z-scan curves (b) of the dispersion of GO in DMF for different input pulse energy with the same pulsewidth τ_p of 4.8 ns. Open-aperture Z-scan curves (c) and NLR Z-scan curves (d) of the dispersion of GO in DMF for different τ_p with the same pulse energy of 5.75μJ (2.54 J/cm^2). $\triangle T_{p\text{-}v}$ (e) and n_{2eff} (f) of dispersions for different τ_p and input pulse energy; Solid lines are theoretical fits. ω_0 = 12μm for (a)- (f).

From Figs. 2(b) and 2(e) we can also see that the difference between normalized transmittance peak and valley ($\Delta T_{P-V} = T_{Peak} - T_{Valley}$) increases as the pulse energy increases. For example, the value of ΔT_{P-V} increases from 0.22 to 0.58 as pulse energy increases from 1.90 μJ (corresponds the input fluence at focus of F_0 = 0.84 J/cm^2) to 8.15 μJ (F_0 = 3.60 J/cm^2) under the same pulsewidth τ_p of 4.8 ns. As shown in Figs. 2(c) and 2(d) the RSA behavior of the dispersion keeps unchanged as τ_p increases with the same input pulse energy (or F_0) at focus. However, the NLR was enhanced for longer pulsewidth. For example, the value of ΔT_{P-V} increases from 0.44 to 1.10 as τ_p increases from 4.8 to 10.7 ns with the same pulse energy of 5.75 μJ (F_0 = 2.54 J/cm^2).

Different mechanisms exist for NLR, such as electronic polarization, molecular reorientation effects, population redistribution (or excited states refraction), free carrier refraction, and thermal effect [26]. In the case of nanosecond pulses, considering the strong linear absorption of the pulse energy for the dispersion, the thermal effect should be generally taken into account for the measurements of NLR. The thermal effect arises from acoustic wave propagation caused by medium density change after local heating, and its buildup time τ_{ac} is determined by the time required for a sound wave to propagate across beam size and $\tau_{ac} = \omega_0/\upsilon_s$, where ω_0 is the beam waist radius and υ_s is the velocity of sound in the medium. Velocity of sound in DMF is υ_s = 1439 m/s [27]. For ω_0 = 12μm, the buildup time of the thermally induced optical nonlinearities τ_{ac} is about 8.3 ns. Since τ_{ac} is comparable to τ_p and the factor τ_p/τ_{ac} is smaller than 1.6, so thermally induced optical nonlinearities is in the transient regime, and acoustic and electromagnetic wave equations must be solved simultaneously in the transient regime while the nonlinear process is simulated numerically [28].

To evaluate the NLR coefficient, we fit the experimental data only by solving the propagation equation of electric field envelope E as Ref. 29, The NLA coefficient and change of refraction index were written as $\alpha(I) = \alpha_0/(1+I/I_S)^{0.5} + \beta_{eff} I$ and $\Delta n(I) = n_{2eff} I$, respectively [12]. Where I is the laser radiation intensity, I_S is saturable intensity, β_{eff} is the effective TPA coefficient. Here an effective NLR coefficient n_{2eff} was used to simplify the multiple nonlinear refraction processes and n_{2eff} values can be obtained by theoretical fitting.

#182213 - $15.00 USD Received 20 Dec 2012; revised 22 Feb 2013; accepted 28 Feb 2013; published 19 Mar 2013

As shown in Fig. 2(f), we can see that $n_{2\text{eff}}$ is negative and the value of $|n_{2\text{eff}}|$ increases from 2.50×10^{-13} to 1.70×10^{-12} cm^2/W as τ_p increases from 4.8 to 10.7 ns with the same pulse energy of 5.75 μJ (F_0 = 2.54 J/cm^2). As the pulse energy increases, the value of $|n_{2\text{eff}}|$ decreases. For example, the $|n_{2\text{eff}}|$ value decreases from 3.52×10^{-13} to 2.32×10^{-13} cm^2/W as input pulse energy from 1.90 μJ (F_0 = 0.84 J/cm^2) to 8.15 μJ (F_0 = 3.60 J/cm^2) with the same pulsewidth τ_p of 4.8 ns. Decreasing $|n_{2\text{eff}}|$ values with increasing input pulse energy indicates that the NLR responses are not arising from intrinsic third-order nonlinear optical response. This phenomenon was also studied in Ref. 30.

The NLR of nigrosine in DMF was also measured, we found that the NLR response and the value of $|n_{2\text{eff}}|$ for the dispersion of GO in DMF were comparable with that for the solution of nigrosine in DMF under the same condition. Since the NLR of nigrosine solution mainly originate from thermal effect [31] and no nonlinear optical signal for DMF was observed in our nanosecond experiments, so the strong pulsewidth influence on NLR indicates the thermal effect exists in the dispersion in nanosecond regime [32]. To further confirm the thermal origin of the NLR, we also measured the NLR of GO under the conditions of two different beam waist radius ω_0 of 12 μm and 22 μm with the same input fluence F_0 at focus. As shown in Figs. 3(a) and 3(b), when ω_0 changes from 12 μm to 22 μm, τ_{ac} increases from 8.3 to 15.3 ns. For τ_p = 10.7 ns, the value of $|n_{2\text{eff}}|$ decreases from 2.26×10^{-12} cm^2/W ($\Delta T_{P-V} = 0.76$) to 8.80×10^{-13} cm^2/W ($\Delta T_{P-V} = 0.54$), with a decreased factor of 2.57 (the ratio of ΔT_{P-V} is 1.41), while for τ_p = 4.8 ns, the value decreases from 2.5 × 10^{-14} cm^2/W ($\Delta T_{P-V} = 0.42$) to 1.3×10^{-14} cm^2/W ($\Delta T_{P-V} = 0.4$), with a decreased factor of 1.92 (1.05). So $|n_{2\text{eff}}|$ (or ΔT_{P-V}) decreases greatly for larger beam waist, which also indicates the existence of thermal effect [31].

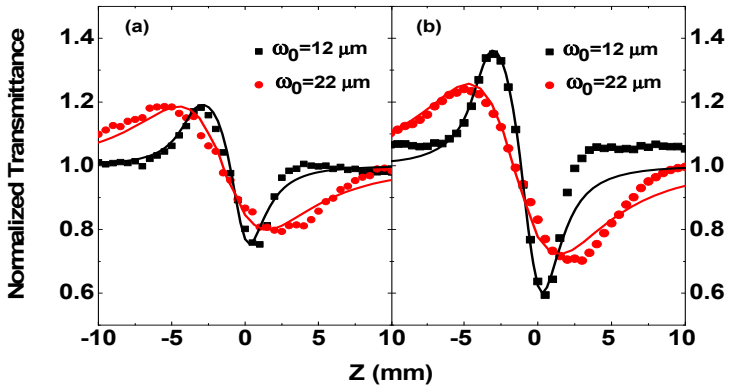

Fig. 3. NLR Z-scan curves of the dispersion of GO in DMF for two different beam waist radius ω_0 for τ_p = 4.8 ns, F_0 = 2.54 J/cm^2. (b) τ_p = 10.7 ns, F_0 = 1.22 J/cm^2. Solid lines are theoretical fits.

SA of the dispersion is attributed to band filling effect of sp^2 domains and RSA can be mainly arising from TPA of sp^3 matrix of GO sheets [7, 8, 12]. By fitting, I_S was obtained to be ~10^7 W/cm^2, β_{eff} to be 3~11.5×10^{-8} cm/W, as τ_p increases from 4.8 to 10.7 ns with the same pulse energy of 5.75 μJ (F_0 = 2.54 J/cm^2), while β_{eff} is near a constant as pulse energy increases with the same τ_p.

Since GO exhibited SA arising from the sp^2 domains, and RSA from the sp^3 matrix in nanosecond, picosecond and femtosecond regime, respectively [7–9, 12], NLR from π electrons and free carriers of sp^2 carbon domains, bound electrons and free carriers of sp^3 matrix may be involved, similar to the case in some semiconductors [33], so NLR response

#182213 - $15.00 USD Received 20 Dec 2012; revised 22 Feb 2013; accepted 28 Feb 2013; published 19 Mar 2013

from GO sheets should not be excluded. However, it is difficult to observe the NLR of GO sheets in nanosecond regime due to strong thermal effect.

To measure the intrinsic NLR of GO sheets, shorter pulses (35 ps) were used. For ω_0 = 16 μm, τ_{ac} = 11.1ns, τ_p/τ_{ac} = 0.003, thus thermal effect can be ignored for the 35 ps pulse. From Figs. 4(a) and 4(b) we can see that GO dispersion shows SA at lower intensity (9.0 GW/cm^2), with further increasing in the intensity, RSA takes place near focus. Since no NLA response of DMF was observed during the open-aperture Z-scan experiments, the SA and RSA behavior should be arising from GO sheets in the dispersion. The fits were obtained by using $I_S = 3.2\text{GW/cm}^2$ and $\beta_{eff} \sim 3.7\times10^{-10}$ cm/W.

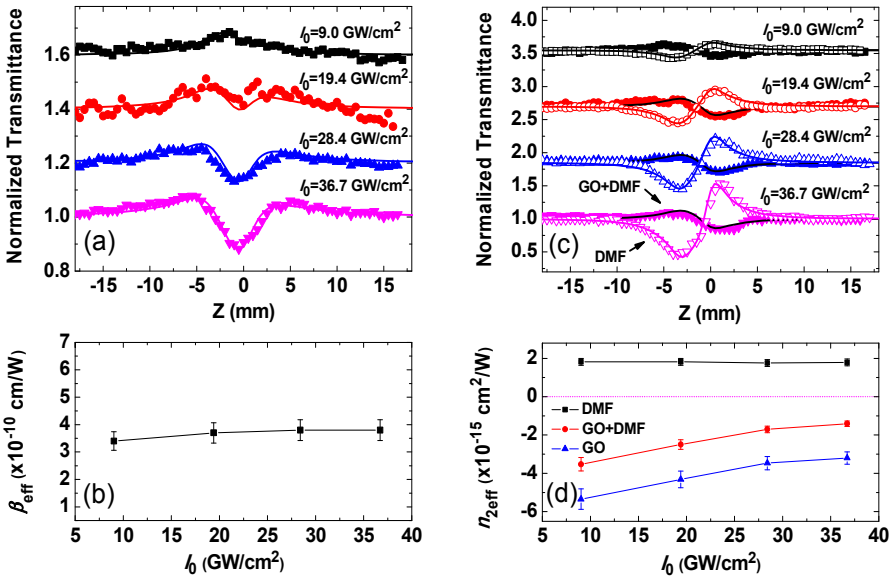

Fig. 4. For 35 ps pulse at 532nm: (a) Open-aperture Z-scan curves of the dispersion of GO in DMF (GO + DMF). (c) NLR Z-scan curves of the dispersion of GO in DMF (GO + DMF) and DMF, solid icons stand for the dispersion (GO + DMF), hollow icons stand for the solvent of DMF. Solid lines are theoretical fits. (b) Effective TPA coefficient β_{eff} of GO as a function of incident intensity. (d) Effective NLR coefficient n_{2eff} of DMF, the dispersion and GO sheets as functions of incident intensity.

For NLR experiments, the NLR properties of solvent DMF cannot be ignored due to the strong peak on-axis intensity I_0 in the sample under picosecond pulse, so the refraction index change Δn (dispersion) for the dispersion can be expressed as $\Delta n\,(\text{dispersion}) = \Delta n\,(\text{GO}) + \Delta n\,(\text{DMF})$, where Δn (GO) is the refraction index change of GO sheets and Δn (DMF) is that of the solvent DMF. Results show that DMF has an intensity-independent positive NLR coefficient n_2 of 1.8×10^{-15} cm^2/W, while GO dispersion (GO + DMF) show negative NLR behaviors arising from GO sheets. As shown in Figs. 4(c) and 4(d), we found that n_{2eff} is negative and the value of $|n_{2eff}|$ of dispersion decreases from 3.5×10^{-15} cm^2/W to 1.4×10^{-15} cm^2/W, as the intensity increases from 9.0 GW/cm^2 to 36.7 GW/cm^2. The value of $|n_{2eff}|$ of GO sheets from calculation decreases from 5.3×10^{-15} cm^2/W to 3.2×10^{-15} cm^2/W. Comparing the open-aperture Z-scan curves in Fig. 4(a) with NLR curves in Fig. 4(c), we note that GO dispersion (and then GO sheets) keeps the negative NLR behaviors though the SA behavior to RSA transition.

Figures 5(a) and 5(c) show the open-aperture Z-scan and NLR curves of the dispersion of GO in DMF under femtosecond pulse laser at 800 nm with different intensity. The results are

#182213 - $15.00 USD Received 20 Dec 2012; revised 22 Feb 2013; accepted 28 Feb 2013; published 19 Mar 2013

similar to the case of picosecond experiments although the laser wavelength and pulse width are different. GO dispersion exhibits SA at lower intensity (82.1 GW/cm^2), with further increase in the intensity, RSA occurs near focus. I_S = 17.5 GW/cm^2 and β_{eff} was about 2.5×10^{-11} cm/W from fitting, as shown in Fig. 5(b). In Fig. 5(d) the results of fits show that DMF has an intensity-independent positive NLR coefficient n_2 of 6.3×10^{-16} cm^2/W. There is a basic agreement with n_2 of DMF in Ref. 21 taking into account the NLR of the quartz cell. We also can see that GO dispersion (GO + DMF) keeps the negative NLR behaviors and the value of $|n_{2\text{eff}}|$ decreases from 5.3×10^{-16} cm^2/W to 4.3×10^{-16} cm^2/W, the calculated value of $n_{2\text{eff}}$ of GO sheets nearly keeps a constant of -1.1×10^{-15} cm^2/W, as intensity increases from 82.1 GW/cm^2 to 224 GW/cm^2. We also should note that GO dispersion (and then GO sheets) keeps the negative NLR behaviors though the SA behavior to RSA transition, similar to the case in picosecond time regime.

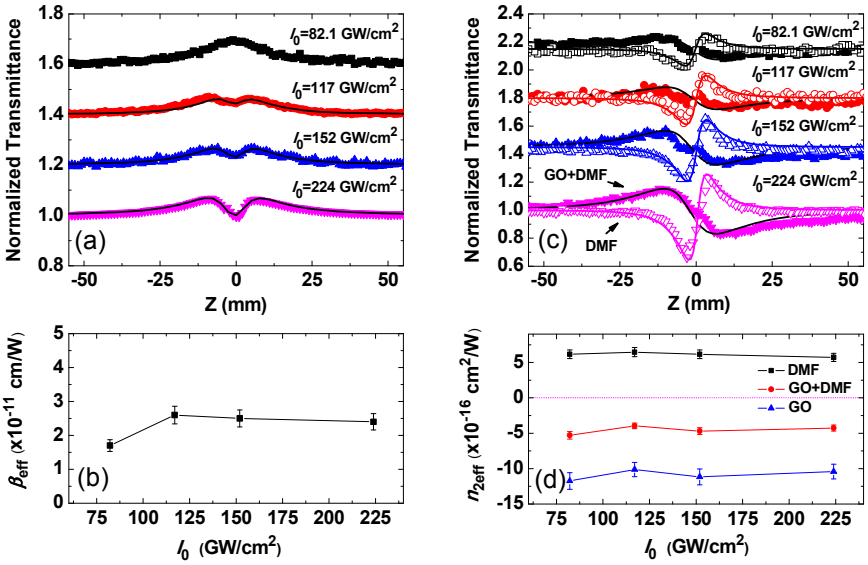

Fig. 5. For 120 fs pulse at 800 nm: (a) Open-aperture Z-scan curves of the dispersion of GO in DMF (GO + DMF). (c) NLR Z-scan curves of the dispersion of GO in DMF (GO + DMF) and DMF, solid icons stand for the dispersion (GO + DMF), hollow icons stand for the solvent of DMF. Solid lines are theoretical fits. (b) Effective TPA coefficient β_{eff} of GO as a function of incident intensity. (d) Effective NLR coefficient $n_{2\text{eff}}$ of DMF, the dispersion and GO sheets as functions of incident intensity.

In femtosecond time regime, electronic polarization, population redistribution (or excited states refraction), free carrier refraction would contribute to the NLR of GO sheets. However, there may be additional molecular reorientation contribution in picosecond and nanosecond time regime. For GO sheets, since the negative NLR were accompanied by SA and RSA in picosecond and femtosecond time regime, the mechanism of NLR from GO sheets can be explained by the schematic drawing shown in Fig. 6. As shown in Fig. 6, the sp^2 domain with a diameter of ~3 nm, has an narrow energy gaps of ~0.5eV [24,34–36], the optical absorption of electrons in sp^2 domains can be saturable easily and SA occur due to valence depletion and conduction band filling. Meanwhile, the π electrons and free carrier refraction in the conduction band of sp^2 domains may contribute to NLR properties.

For sp^3 matrix, the energy gaps are large (typically 2.7~3.1 eV) [37], when the intensity of laser pulse increases, the bound electrons in the valence band in sp^3 matrix will transit to conduction band and become free carriers through TPA mechanism for 532nm or 800 nm

#182213 - $15.00 USD Received 20 Dec 2012; revised 22 Feb 2013; accepted 28 Feb 2013; published 19 Mar 2013

pulse laser. Since the relaxation time of free carriers are in the order of hundreds of femtosecond, and a few picoseconds to scores of picoseconds [8], the bound electron NLR in the valence band and free carrier refraction in the conduction band of sp^3 matrix will also contribute to the NLR response of GO sheets. In GO sheets, sp^2 domains and sp^3 matrix are coexistence, so SA, TPA and possible free carrier absorption (FCA) are coexistence in a GO sheet. In femtosecond time regime, the NLR from π electrons, bound electrons in the valence band and free carriers in the conduction band will contribute to the NLR of the whole GO sheets. What' more, in the time regime of picosecond or longer, molecular reorientation effects of GO sheets may be also involved. While in nanosecond time regime, the contribution of these processes can be neglected because of the dominant transient thermal effect.

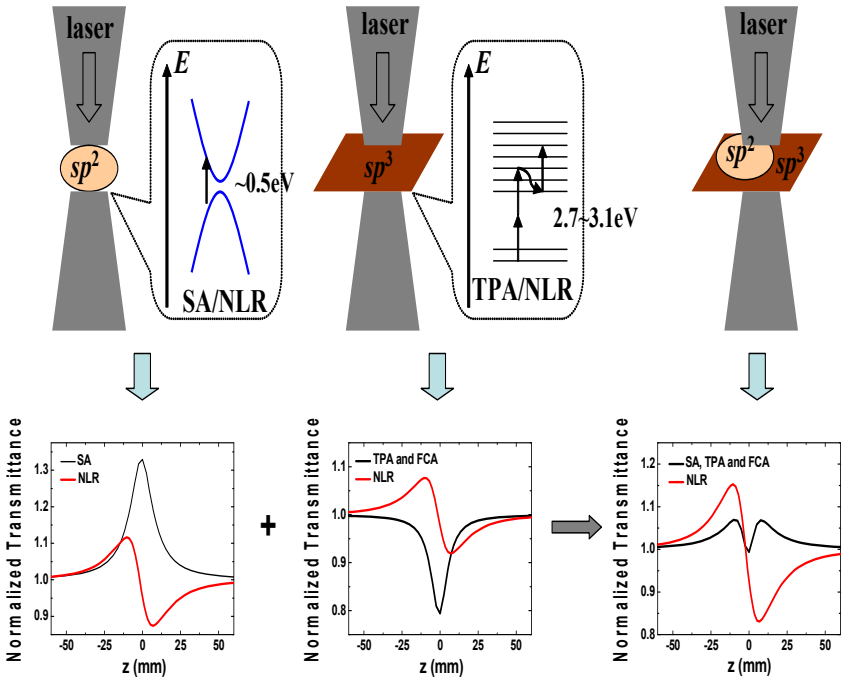

Fig. 6. A schematic drawing of NLA and NLR arising from sp^2 domains and sp^3 matrix of GO sheets.

It should be pointed out that there are many differences in NLR mechanisms between the graphene layer on a substrate, graphene sheets in solution dispersions and GO sheets in dispersions. For single layer or few-layer graphene on a substrate, the NLR from π electrons is dominant and NLR are not affected by cumulative thermal effect due to the very high thermal diffusion coefficient of graphene [15]. For graphene sheets in solution dispersions, both π electrons and the reorientation and alignment of the graphene sheets can contribute to the NLR [13, 14], thermal effect from solution dispersions can also contribute to NLR under continuous wave or long pulse laser. For GO sheets in dispersions, free carriers, π electrons and bound electrons of sp^2 domains and sp^3 matrix can contribute to the NLR. Reorientation effects of the GO sheets and thermal effect should be considered according to the duration of pulse.

Moreover, unlike the case of single layer or few-layer graphene on a substrate, the NLR response and $n_{2\text{eff}}$ value of graphene sheet or GO sheets dispersions is the sum of NLR signals from a large amount of sheets interacting with laser pulse. The NLR response or $n_{2\text{eff}}$ value of single graphene sheet or GO sheet cannot be obtained accurately, only can be obtained by

#182213 - $15.00 USD Received 20 Dec 2012; revised 22 Feb 2013; accepted 28 Feb 2013; published 19 Mar 2013

roughly qualitative estimation [13], because the sheets are dispersed and the sheets sizes are not uniform. So the values of $n_{2\text{eff}}$ (or n_2) in the three cases, cannot be compared directly, because the duration of laser pulse and wavelength, the samples and the mechanisms contributing to NLR are different.

4. Conclusions

In summary, the NLR properties of GO in DMF were studied in nanosecond, picosecond and femtosecond time regimes by Z-scan technique, NLA properties related to NLR properties were also studied. Results show that the dispersion of GO in DMF exhibit negative NLR properties, which is mainly attributed to transient thermal effect in nanosecond time regime. GO dispersions also exhibits negative NLR in picosecond and femtosecond time regime, which may be mainly arising from electronic polarization and possible free carrier refraction of sp^2 domains and sp^3 matrix of GO sheets. GO dispersions and GO sheets keep negative NLR behaviors although the SA behaviors to RSA transition as pulse energy (intensity) increases in nanosecond, picosecond and femtosecond regimes, this makes GO materials promising candidates for practical applications as broadband and broad domain saturable absorbers, optical switching and optical limiter.

Acknowledgments

The authors thank Xiao-Qing Yan of Nankai University for the helpful discussion. This work was supported by the Program for New Century Excellent Talents in University (NCET-09-0484), Youth Foundation of Taiyuan University of Technology (No. 2012L085), and the Scientific Research Starting Foundation from Taiyuan University of Technology.

#182213 - $15.00 USD Received 20 Dec 2012; revised 22 Feb 2013; accepted 28 Feb 2013; published 19 Mar 2013